



HAL
open science

Investigating 2M1155-79B: A Nearby, Young, Low-mass Star Actively Accreting from a Nearly Edge-on, Dusty Disk

D. Annie Dickson-Vandervelde, Joel H. Kastner, Jonathan Gagné, Adam C. Schneider, Jacqueline Faherty, Emily C. Wilson, Christophe Pinte, Francois Ménard

► To cite this version:

D. Annie Dickson-Vandervelde, Joel H. Kastner, Jonathan Gagné, Adam C. Schneider, Jacqueline Faherty, et al.. Investigating 2M1155-79B: A Nearby, Young, Low-mass Star Actively Accreting from a Nearly Edge-on, Dusty Disk. *The Astronomical Journal*, 2022, 164, 10.3847/1538-3881/ac9674 . insu-03860261

HAL Id: insu-03860261

<https://insu.hal.science/insu-03860261>

Submitted on 19 Nov 2022

HAL is a multi-disciplinary open access archive for the deposit and dissemination of scientific research documents, whether they are published or not. The documents may come from teaching and research institutions in France or abroad, or from public or private research centers.

L'archive ouverte pluridisciplinaire **HAL**, est destinée au dépôt et à la diffusion de documents scientifiques de niveau recherche, publiés ou non, émanant des établissements d'enseignement et de recherche français ou étrangers, des laboratoires publics ou privés.



Distributed under a Creative Commons Attribution 4.0 International License



Investigating 2M1155–79B: A Nearby, Young, Low-mass Star Actively Accreting from a Nearly Edge-on, Dusty Disk

D. Annie Dickson-Vandervelde^{1,2} , Joel H. Kastner^{1,2,3} , Jonathan Gagné^{4,5} , Adam C. Schneider^{6,7} , Jacqueline Faherty⁸ , Emily C. Wilson^{1,9} , Christophe Pinte¹⁰ , and Francois Ménard¹¹

¹School of Physics and Astronomy, Rochester Institute of Technology, Rochester, NY 14623, USA; dad1197@rit.edu

²Laboratory for Multiwavelength Astrophysics, Rochester Institute of Technology, Rochester, NY 14623, USA

³Center for Imaging Science, Rochester Institute of Technology, Rochester, NY 14623, USA; jhk@cis.rit.edu

⁴Planétarium Rio Tinto Alcan, Espace pour la Vie, 4801 av. Pierre-de Coubertin, Montréal, Québec, Canada

⁵Institute for Research on Exoplanets, Université de Montréal, Département de Physique, C.P. 6128 Succ. Centre-ville, Montréal, QC H3C 3J7, Canada

⁶United States Naval Observatory, Flagstaff Station, 10391 West Naval Observatory Road, Flagstaff, AZ 86005, USA

⁷Department of Physics and Astronomy, George Mason University, MS3F3, 4400 University Drive, Fairfax, VA 22030, USA

⁸Department of Astrophysics, American Museum of Natural History, Central Park West at 79th Street, New York, NY 10024, USA

⁹Center for Computational Relativity and Gravitation, Rochester Institute of Technology, Rochester, NY 14623, USA

¹⁰Monash Centre for Astrophysics (MoCA) and School of Physics and Astronomy, Monash University, Clayton, Vic 3800, Australia

¹¹Univ. Grenoble Alpes, CNRS, IPAG, F-38000 Grenoble, France

Received 2022 May 13; revised 2022 September 28; accepted 2022 September 28; published 2022 October 31

Abstract

We investigate the nature of an unusually faint member of the ϵ Cha association ($D \sim 100$ pc, age ~ 5 Myr), the nearest region of star formation of age < 8 Myr. This object, 2MASS J11550336–7919147 (2M1155–79B), is a wide-separation (~ 580 au), comoving companion to low-mass (M3) ϵ Cha association member 2MASS J11550485–7919108 (2M1155–79A). We present near-infrared (NIR) spectra of both components, along with analysis of photometry from Gaia Early Data Release 3, the Two Micron All Sky Survey, the Vista Hemisphere Survey, and the Wide-field Infrared Survey Explorer (WISE). The NIR spectrum of 2M1155–79B displays strong He I 1.083 emission, a sign of active accretion and/or accretion-driven winds from a circumstellar disk. Analysis of WISE archival data reveals that the mid-infrared excess previously associated with 2M1155–79A instead originates from the disk surrounding 2M1155–79B. Based on these results, as well as radiative transfer modeling of its optical/IR spectral energy distribution, we conclude that 2M1155–79B is most likely a young, late M star that is partially obscured by, and actively accreting from, a nearly edge-on circumstellar disk. This would place 2M1155–79B among the rare group of nearby ($D \lesssim 100$ pc), young (age < 10 Myr) mid-M stars that are orbited by and accreting from highly inclined protoplanetary disks. Like these systems, the 2M1155–79B system is a particularly promising subject for studies of star and planet formation around low-mass stars.

Unified Astronomy Thesaurus concepts: [Protoplanetary disks \(1300\)](#); [Pre-main sequence stars \(1290\)](#)

Supporting material: data behind figure

1. Introduction

Nearby associations of young, comoving stars (generally referred to as nearby young moving groups (NYMGs)) are prime candidates for studies of the early evolution of low-mass pre-main-sequence (pre-MS) stars, juvenile brown dwarfs, and newly formed planets (Kastner et al. 2016; Gagné & Faherty 2018). In recent years there have been a handful of identifications of very wide (~ 100 – 1000 au projected separation) binaries consisting of young stars and substellar objects in these NYMGs, as well as in nearby star formation regions (HD 106906 b, IRXS 160929.1–210524 B, CT Cha B, and DENIS-P J1538317–103850; Wu et al. 2015a, 2015b, 2016; Nguyen-Thanh et al. 2020).

The faint Two Micron All Sky Survey (2MASS) source 2MASS J11550336–79191147 (henceforth 2M1155–79B) is a curious young, low-mass object that was discovered via a Gaia Data Release 2 (DR2; Gaia Collaboration et al. 2016) search for wide, comoving companions to known members of the ϵ Cha association (ϵ CA; $D \sim 100$ pc, age ~ 5 Myr), which represents the nearest region of star formation of age < 8 Myr

(Dickson-Vandervelde et al. 2020, 2021). 2M1155–79B is the companion to 2MASS J11550486–7919108 (henceforth 2M1155–79A) with a projected separation of $5''.75$, equivalent to 582 au at position angle (PA) $227^\circ.9$ (Murphy et al. 2013; Dickson-Vandervelde et al. 2020). Astrometry from Gaia Early Data Release 3 (EDR3) confirms that 2M1155–79A and 2M1155–79B are equidistant ($D = 101.4 \pm 0.3$ pc; Bailer-Jones et al. 2021) and comoving, to within the uncertainties (Table 1). The M3-type star 2M1155–79A was previously known as T Cha B, following its identification as an apparent very wide separation comoving companion to T Cha, host to one of the nearest known examples of a highly inclined protoplanetary disk (Kastner et al. 2012). However, Gaia DR2 subsequently revealed small but statistically significant differences between the parallaxes and proper motions of T Cha and 2M1155–79A (Kastner 2018).¹²

Using substellar object population properties, Dickson-Vandervelde et al. (2020) found that the J magnitude and $J-H$ color of 2M1155–79B corresponded to a spectral type of M9/L0, which would place it just below the boundary between brown dwarfs and massive planets assuming that its age is 5 Myr. This mass estimate would place 2M1155–79B in the interesting

Original content from this work may be used under the terms of the [Creative Commons Attribution 4.0 licence](#). Any further distribution of this work must maintain attribution to the author(s) and the title of the work, journal citation and DOI.

¹² Gaia EDR3 data appear to confirm that T Cha and 2M1155–79A are neither equidistant nor comoving (within the uncertainties).

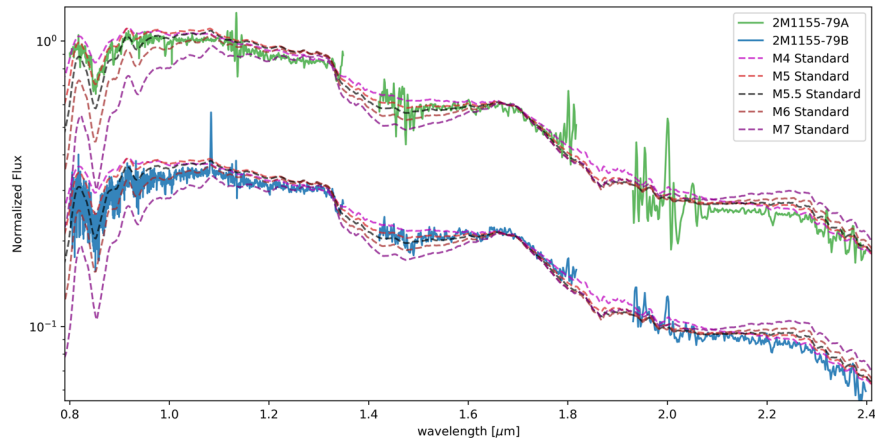


Figure 1. NIR spectra obtained with the FIRE instrument on Magellan for 2M1155–79A (green) and 2M1155–79B (blue). The fluxes of both FIRE spectra have been normalized and a constant offset applied to 2M1155–79B, for purposes of visualization. Five spectra from the Luhman et al. (2017) Young Star Spectral Library, M4 (magenta), M5 (red), M5.5 (black), M6 (brown), and M7 (purple), are also displayed, with intensities adjusted to match the FIRE spectra at 1.7 μm .

(The data used to create this figure are available.)

Table 1
2M1155–79AB: Gaia EDR3 Astronomy and Photometry

Name	R.A. (deg)	Decl. (deg)	π (mas)	PMRA (mas yr ⁻¹)	PMDec (mas yr ⁻¹)	G (mag)	$G-G_{\text{RP}}$ (mag)	RUWE
2M1155–79A	178.769132	–79.319756	9.81 \pm 0.03	–41.35 \pm 0.03	–4.56 \pm 0.031	14.803	1.333	1.196
2M1155–79B	178.762736	–79.320829	9.49 \pm 0.43	–41.59 \pm 0.55	–4.63 \pm 0.51	19.954	1.396	1.104

position of a planet orbiting its host (2M1155–79A) at a projected semimajor axis of ~ 600 au—similar to the projected separations of the aforementioned substellar-object-hosting systems HD 106906, IRXS 160929.1–210524, CT Cha, and DENIS-P J1538317–103850. The formation mechanisms of such wide-orbit massive planets remain subject to debate; proposed methods of formation range from dynamical interactions to standard star formation mechanisms (e.g., Lagrange et al. 2016; Rodet et al. 2019; Lodieu et al. 2021).

In this paper, we present near-infrared (NIR) spectroscopy of the 2M1155–79AB system, along with analysis of available Gaia EDR3, 2MASS, and Wide-field Infrared Survey Explorer (WISE) photometry. The results suggest a different nature for 2M1155–79B: namely, that it is a low-mass pre-MS star partially occulted by, and actively accreting from, a highly inclined, dusty disk. In Section 2, we describe the NIR spectroscopic observations. In Section 3, we present the results of these observations, along with analysis of archival photometry of the 2M1155–79AB system. In Section 4, we discuss the evidence for a disk around 2M1155–79B and compare the object to 2M1155–79A. We also compare the 2M1155–79B star–disk system to a set of potentially analogous very low mass star–disk systems: fellow ϵ CA member 2MASS J12014343–7835472, member of the 8 Myr TW Hya association TWA 30B, and the 1–5 Myr old DENIS-P J1538317–103850.

2. Observations

NIR spectra were obtained on 2020 February 12 and 13 (hereafter Night 1 and Night 2, respectively) using the FIRE instrument on the 6.5 m Magellan telescope. FIRE spectra were obtained in prism mode, which has a resolving power of ~ 450 across the 0.8–2.5 μm spectral range. Observations of 2M1155

–79B were obtained on both nights, and observations of 2M1155–79A were obtained on Night 2 (Figure 1).

The FIRE data were reduced using a custom version of the FIREHOSE pipeline based on the MASE pipeline (Bochanski et al. 2009) written in the Interactive Data Language (IDL).¹³ This modified version includes subroutines of the SpexTool package (Vacca et al. 2003; Cushing et al. 2004) to facilitate the rejection of bad pixels and detector hot spots with the 1D extracted spectra of individual exposures. All raw exposures were flat-fielded, then extracted using the optimal extraction algorithm included in FIREHOSE, and finally combined using the default Robust Weighted Mean option (Robust threshold = 8.0). We used neon-argon lamp exposures to determine the wavelength calibration. The signal-to-noise ratio (S/N) per resolution element is approximately 180 (70 pixel⁻¹) for 2M1155–79B and about 260 (100 pixel⁻¹) for 2M1155–79A.

While the overall shape and features of the spectra for 2M1155–79B did not change between Night 1 and Night 2, the spectrum obtained on Night 1 displays lower S/N, especially in the ~ 2 μm region. Hence, the analysis and discussion in this paper refer to the Night 2 spectrum, unless otherwise specified.

The majority of ϵ CA members show no significant intervening reddening (Murphy et al. 2013), consistent with the general lack of extinction in the direction of the group ($E(B-V) < 0.03$) out to distances of ~ 160 pc (Lallement et al. 2019). However, the 2M1155–79AB system (like neighboring T Cha) is seen projected toward the middle of a small dust cloud (Murphy et al. 2013; Sacco et al. 2014). Hence, the spectra of both components were dereddened via the Python package `dust_extinction` using the Fitzpatrick et al. (2019) reddening model. We adopted $E(B-V) = 0.5$ for 2M1155–79A (Murphy et al. 2013), which equates

¹³ Available at https://github.com/jgagneastro/FireHose_v2.

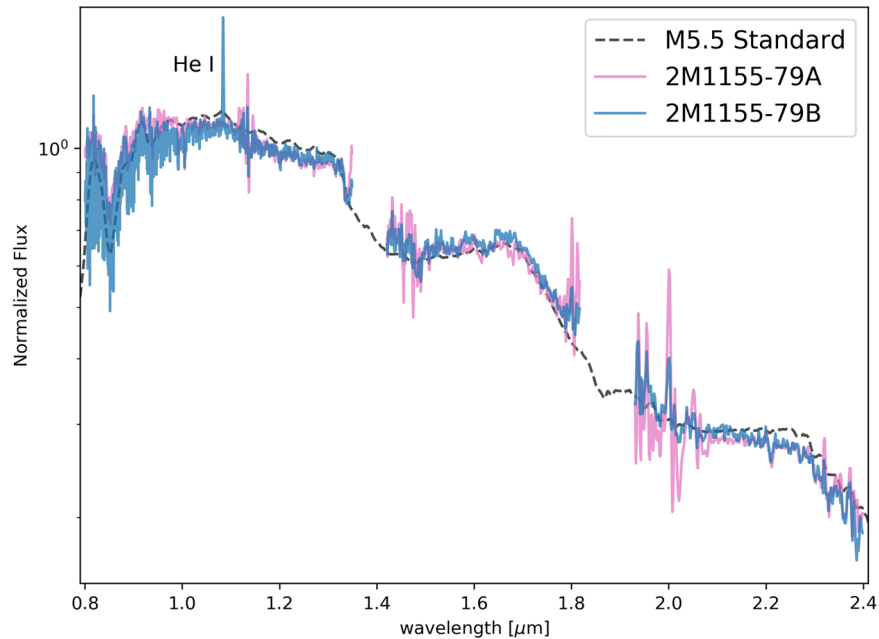


Figure 2. NIR spectra of 2M1155–79A (green), 2M1155–79B (blue), and an M5.5 standard (dashed black), displayed with fluxes normalized to the value at $0.85 \mu\text{m}$. Aside from the $1.083 \mu\text{m}$ He I emission line seen in 2M1155–79B, no other emission lines are detected in either star. Notably, the two companions have very similar morphologies with the exception of the He I emission line.

to $A_J \approx 0.44$, assuming the standard value of $R_V = 3.1$ (e.g., Cardelli et al. 1989). Note that this dereddening process does not account for other sources of spectral distortion, such as obscuration or scattering by circumstellar disk material.

3. Results

3.1. NIR Spectra

In Figure 1, we present the dereddened Magellan/FIRE spectra for both 2M1155–79A and 2M1155–79B overlaid with a range of NIR spectra of late M young star spectral standards from Luhman et al. (2017, hereafter L17). Before normalizing the two spectra, the 2M1155–79A spectrum is on average $10.2\times$ brighter than its companion. After accounting for this factor of 10 difference in flux, the spectral shapes of 2M1155–79A and 2M1155–79B are very similar, with some small differences in the depth of the $0.8 \mu\text{m}$ absorption feature that could be due to noise (see the two spectra overlaid in Figure 2). The $1.4\text{--}1.8 \mu\text{m}$ region of the spectrum of 2M1155–79B also potentially shows a larger bump than that of 2M1155–79A, and 2M1155–79B appears slightly redder than 2M1155–79A in the $0.8\text{--}1.1 \mu\text{m}$ region, indicative of a slightly later spectral type. Notably, the spectrum of 2M1155–79B displays a strong $1.083 \mu\text{m}$ He I emission feature that is absent from the spectrum of 2M1155–79A.

The overall strong similarity of the Magellan/FIRE spectrum of 2M1155–79B to that of 2M1155–79A indicates that the two components are very similar in spectral type, notwithstanding the factor ~ 10 smaller spectral flux from 2M1155–79B. As is discussed in detail below, this is a surprising result, given that (as noted) 2M1155–79A has been classified as M3 (Kastner et al. 2012; Murphy et al. 2013), whereas 2M1155–79B was initially considered a candidate substellar object (Dickson-Vandervelde et al. 2020). Additionally, while the comparison of the NIR spectra of the 2M1155–79AB pair with the L17 standard spectra in Figure 1 does leave some ambiguity as to the M spectral subtypes

of 2M1155–79A and 2M1155–79B, it is readily apparent that the NIR spectral type of the former component is later than M3.

The comparison of the overall shapes of the FIRE spectra with those of the L17 young star standard spectra demonstrates that a spectral type of M7 or later can be ruled out; note in particular the flatter slope of both 2M1155–79A and B in the $1.4\text{--}1.8 \mu\text{m}$ and $1.9\text{--}2.4 \mu\text{m}$ regions relative to the M7 standard. The $2.2 \mu\text{m}$ Na I absorption line is present in both FIRE spectra, although it is not present in the standards, and the line depth is in agreement with a mid- to late M spectral type. The $0.8\text{--}0.9 \mu\text{m}$ range of 2M1155–79B has a lower S/N than other regions of the spectrum, and so the TiO feature matches with a larger range of spectral types; 2M1155–79A is less noisy in that range and more precisely matches to the M5–M6 standard. Again, the slope of the M7 standard is more pronounced than either 2M1155–79A or B. Hence, a spectral type in the range of M5–M6 is the best match for both 2M1155–79A and B.

3.1.1. The He I Feature

Both (Night 1 and 2) spectra of 2M1155–79B data show the presence of a strong He I $1.083 \mu\text{m}$ emission line (Figure 2). The emission line is unresolved, placing an upper limit of $\sim 670 \text{ km s}^{-1}$ on its velocity width. The equivalent widths (EWs) of the $1.083 \mu\text{m}$ emission line, as measured via Gaussian fitting, were $-11.9 \pm 0.6 \text{ \AA}$ and $-12.6 \pm 0.4 \text{ \AA}$ for the Night 1 and 2 spectra, respectively.

3.1.2. Low-gravity Features

We analyzed the 2M1155–79B spectrum for potential spectral features that are sensitive to stellar surface gravity and useful for gravity indexing spectral types of M6 and later (Allers & Liu 2013, and references therein). Both the 1.14 and $2.21 \mu\text{m}$ Na I absorption lines are visible, consistent with a mid-/late M classification (see above); the Na I feature is not present in lower-mass objects. The three FeH features (0.99 ,

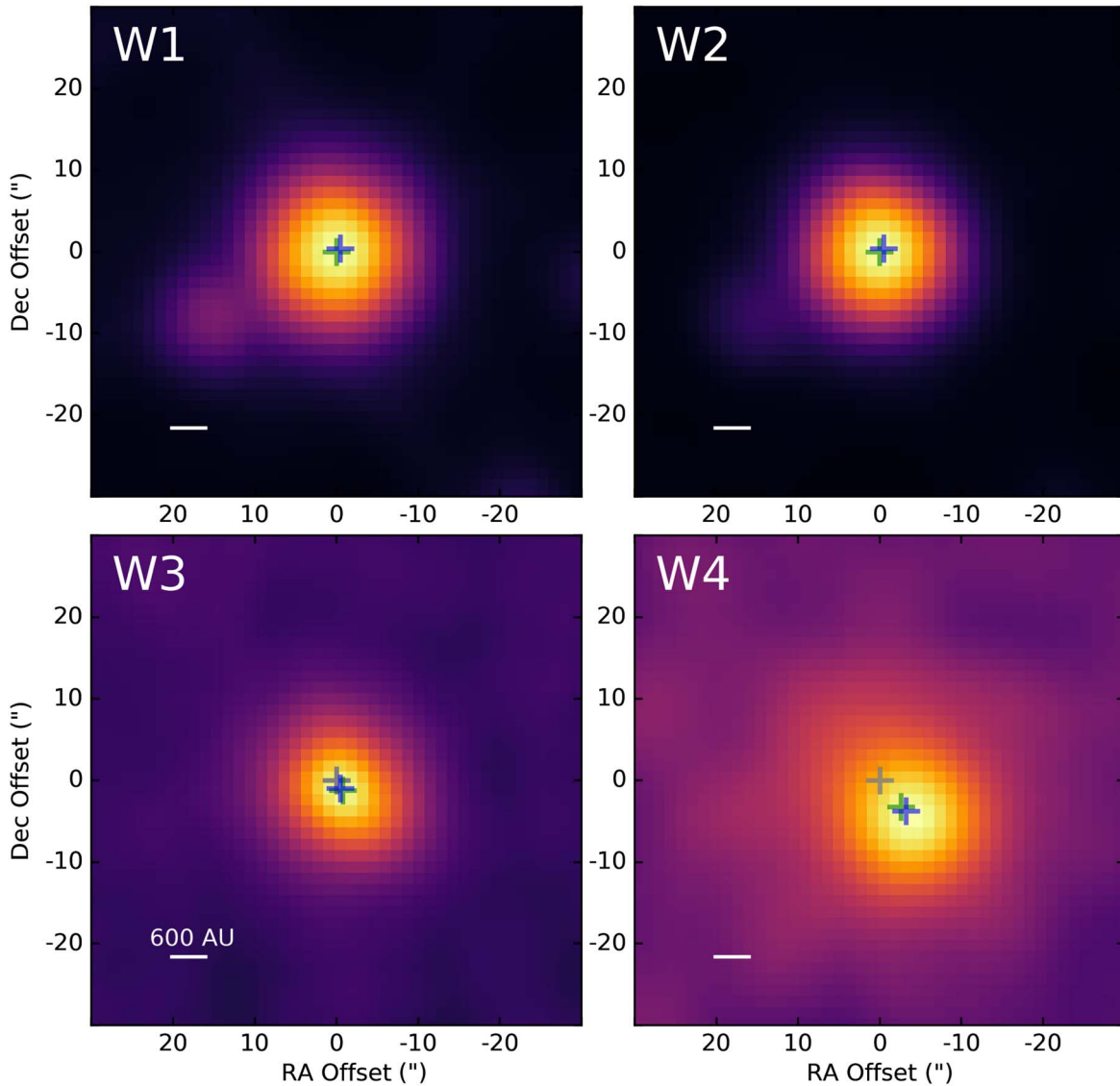


Figure 3. Four WISE archival log-scaled images of the 2M1155–79AB system, W1, W2, W3, and W4 (3.6, 4.5, 12, and 22 μm) as labeled. Images are aligned in R.A./decl. coordinates, (0,0) being the position of the W1 centroid, and are $60'' \times 60''$. The white bar on each image represents the equivalent distance of ~ 600 au, the green plus sign marks the center of the PSF as found via a Gaussian, the blue plus sign marks the center of the PSF as found via the peak pixel value, and the gray plus sign in the W3 and W4 images marks the W1 (0,0) position.

1.20, and 1.55 μm) are not detected at the current S/N; this is in agreement with the morphological spectral type of M5–M6 for 2M1155–79B indicated by Figure 1, as deeper FeH spectral lines are indicative of later (late M to early L) spectral types.

3.2. WISE Image Centroids

Mid-infrared 3.6, 4.5, 12, and 22 μm (W1, W2, W3, W4 band) images of the 2M1155–79AB binary system obtained by WISE are presented in Figure 3. The angular resolution of WISE is comparable to the 2M1155–79AB system separation ($\sim 6''$); however, it is apparent that the source centroid shifts from W1 (3.6 μm) to W4 (22 μm) by a displacement similar to this angular offset. In order to determine which component dominates each WISE band, we performed a centroid analysis on all four WISE images and calculated the shift of center of the point-spread function (PSF). We used two methods to determine the center of the WISE emission: Gaussian PSF centroid fitting and peak pixel

position determination. The two methods yield the same results to within the uncertainties (Figure 3). Analysis of unWISE data (Schlafly et al. 2019) yields similar results. Considering the spectral energy distribution (SED) morphologies of 2M1155–79A and 2M1155–79B (see Section 3.3, Figure 4), the majority of the flux in W1 is presumed to be from 2M1155–79A; thus, we consider the photocenter found via our analysis of the W1 image to be the position of 2M1155–79A.

The measured offsets with respect to W1 are $0''.03$ (PA = 270°), $1''.44$ (PA = 242°), and $4''.14$ (PA = 229°) in the W2, W3, and W4 band images, respectively. The W4 angular offset and PA, relative to W1, are similar to the projected separation ($5''.75$) and PA (227°) of 2M1155–79B, relative to 2M1155–79A (Dickson-Vandervelde et al. 2020). We conclude that 2M1155–79A dominates the flux in the shorter WISE bands (W1 and W2), while the contribution from 2M1155–79B becomes significant at 12 μm (W3) and dominates the flux at 22 μm (W4). Thus, the mid-IR excess due to thermal emission from circumstellar dust—originally attributed to 2M1155–79A (Kastner et al. 2012;

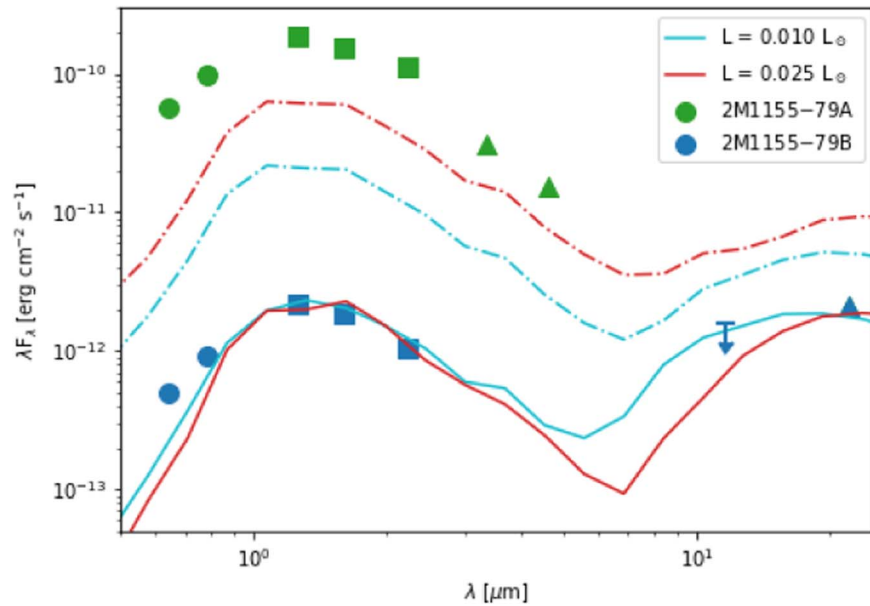


Figure 4. The SED of 2M1155–79B (blue symbols) with two MCFOST models overlotted; the SED of 2M1155–79A (green symbols) is also plotted as a reference. Circles represent fluxes from Gaia EDR3 (G and G_{RP}), squares represent fluxes from 2MASS (J , H , and K), and triangles represent fluxes from WISE (W1, W2, W3, and W4). The J and K fluxes for 2M1155–79B are from VHS. The WISE fluxes are partitioned according to which object clearly dominates in each band; the downward-pointing arrow represents the upper limit on the W3 flux for 2M1155–79B, since it is not clear how much this source contributes to the emission in this WISE band (see Section 3.2). The cyan line is the highly inclined model corresponding to a stellar luminosity of $0.010 L_{\odot}$, and the red line is the highly inclined model corresponding to $0.025 L_{\odot}$. The dashed–dotted lines correspond to the respective pole-on models for 0.010 and $0.025 L_{\odot}$.

Murphy et al. 2013)—is in fact associated with 2M1155–79B (see next).

3.3. SEDs

In addition to photometry from WISE (Wright et al. 2010), archival photometry is available for both 2M1155–79B and 2M1155–79A from Gaia EDR3 (Gaia Collaboration et al. 2021), 2MASS (Skrutskie et al. 2006), and the Vista Hemisphere Survey (VHS; McMahon et al. 2013). The visible and NIR magnitudes were dereddened for 2M1155–79A and 2M1155–79B following the same procedure used for the FIRE spectra (see Section 2). The resulting SEDs generated from these archival data are presented in Figure 4. Throughout the optical and mid-IR SED, there is a factor of ~ 100 luminosity difference between A and B. This is discrepant with the NIR flux ratio seen in the FIRE data (~ 10). Although the flux ratio measured in the FIRE spectra may be unreliable, due to possible chromatic effects from slit placement and possible saturation in the J -band portions of the spectra of 2M1155–79A and the (A0) flux calibration standard, the large discrepancy between the 2MASS flux ratios and the FIRE spectral ratio is indicative of possible variable obscuration of 2M1155–79B (see below).

The W1–W2 color of 2M1155–79A (0.23 ± 0.03) is consistent with that expected from photospheric emission for a star in its (mid-M) spectral type range (i.e., for M5 and M6, W1–W2 = 0.21 and 0.27, respectively; Pecaut & Mamajek 2013). Additionally, the W4 ($22 \mu\text{m}$) flux arises primarily from 2M1155–79B (Section 3.2). Therefore, we find no evidence for a warm circumstellar dust component associated with 2M1155–79A.

4. Discussion

4.1. The Two Components of 2M1155–79

As noted in Section 3.1, the NIR SED revealed by the FIRE spectra of 2M1155–79B is strikingly similar to—albeit significantly fainter than—that of 2M1155–79A (Figure 1). In addition to the large flux ratio, a glaring distinction between the two spectra is the presence of the He I $1.083 \mu\text{m}$ emission line in 2M1155–79B. The WISE analysis reveals that the IR excess originally associated with 2M1155–79A instead arises from 2M1155–79B (see Section 3.2). This, combined with the He I emission, constitutes strong evidence for the presence of a disk surrounding, and accreting onto, 2M1155–79B. Edge-on disks appear unusually faint in optical and NIR bands compared to the expected luminosities of a given spectral type, while still presenting an IR excess at longer wavelengths. This is because the stellar photosphere is occulted, such that photospheric radiation that is scattered off of the disk surface dominates the optical and NIR SED (accounting for the diminished flux in that regime), while thermal IR emission from the disk dust still emerges (e.g., D’Alessio et al. 2006; Furlan et al. 2011). The very low apparent luminosity and red Gaia/2MASS colors of 2M1155–79B (Dickson-Vandervelde et al. 2020) hence could be due to obscuration of the stellar photosphere by this orbiting, dusty accretion disk.

As an initial investigation of this hypothesis, we used the radiative transfer modeling code MCFOST (Pinte et al. 2006, 2009) to generate two models for the combined star and disk system of 2M1155–79B that can reproduce its double-peaked optical through mid-IR SED, as illustrated in Figure 4. These models represent two extremes of stellar luminosity, 0.010 and $0.025 L_{\odot}$, with the stellar effective temperature fixed at 3000 K using the Baraffe et al. (2015) stellar spectra models, corresponding to the expected range of stellar

properties for ~ 5 Myr old M5/M6 pre-MS stars. For both scenarios, we utilized a tapered-edge disk model composed of astronomical silicates—separated into small ($0.01\text{--}7\ \mu\text{m}$) and large ($7\text{--}3000\ \mu\text{m}$) grains—with a flaring exponent of 1.07 and a disk scale height of 7 au at a reference radius of 100 au (Pinte et al. 2009). We fixed the large grain dust disk mass at $2.0 \times 10^{-5} M_{\odot}$ and the small grain dust disk mass at $1.5 \times 10^{-6} M_{\odot}$. The small dust grain component remained the same between both models with an inner radius of 0.015 au and outer radius of 60 au. To match the observed SED, we find that the $0.010 L_{\odot}$ model requires a disk inclination of 75° and an inner radius of 0.2 au for the large dust grains, while the $0.025 L_{\odot}$ model requires an inclination of 81° and an inner radius of 0.45 au for the large dust grains. We also display the corresponding models for an inclination of 0° (i.e., pole-on) in Figure 4; these models support the conclusion that obscuration by the disk is responsible for the observed weak stellar photospheric emission signature in the 2M1155–79B SED. These initial MCFOST modeling results (Figure 4) thus lend strong support to the scenario wherein the observed SED of 2M1155–79B results from a highly inclined circumstellar disk.

In contrast, given the WISE data (and lack of He I emission from 2M1155–79A), we can now conclude that there is no evidence for a circumstellar disk around 2M1155–79A. The NIR spectra (Figure 1) indicate that both 2M1155–79A and B are mid- to late M (M5/6) type stars, whereas optical spectroscopy of 2M1155–79A previously established the star as spectral type M3 (Kastner et al. 2012). The discrepancy between these NIR (M5/6) and optical (M3) spectral classifications would not be without precedent; it has been previously noted that the optical spectral classifications of pre-MS stars can be three to five subclasses earlier than their NIR-based classifications (Kastner et al. 2015; Pecaut 2016). However, it is possible that the previous determination of an earlier spectral type for 2M1155–79A could reflect the relatively limited wavelength range of the spectrum used for classification.

Furthermore, our MCFOST modeling demonstrates that the occultation of 2M1155–79B by this disk—rather than a difference in stellar mass (hence luminosity)—also most likely accounts for much of the enormous flux difference between 2M1155–79B and 2M1155–79A throughout the optical and NIR. The strong similarity of the FIRE spectra of 2M1155–79A and 2M1155–79B, as well as their factor ~ 10 difference in flux levels, should translate to very similar 2MASS colors and a systematic difference of ~ 2.5 mag in the 2MASS photometry. The redder 2MASS $J - H$ color of 2M1155–79B, and the overall ~ 5 mag difference between the two components in the 2MASS data, hence strongly suggests that, at the epoch of 2MASS (1998), 2M1155–79B was more heavily occulted by its disk than when we observed in 2020. Such variable obscuration is frequently observed in analogous highly inclined star/disk systems (see Section 4.2). On the other hand, the fact that the Gaia EDR3 $G - G_{\text{RP}}$ color of 2M1155–79B is not as red as in the DR2 photometry ($G - G_{\text{RP}} = 1.40$ and 1.74 , respectively) is more likely due to a spurious measurement of G_{RP} in DR2. Such Gaia color variability would seem to be inconsistent with the very highly inclined ($i \sim 80^{\circ}$), optically thick disk invoked in our models; the photospheric component in these models is dominated by scattering, such that the optical/NIR colors should be saturated and (hence) constant. Additional photometric monitoring of this system, along the lines of that conducted for TWA 30AB (see next), is clearly warranted.

4.2. Comparison to Analogous Systems

Various young, low-mass star/disk systems, some of them also binaries, provide useful points of comparison with the 2M1155–79AB system. Two particularly interesting objects for purposes of comparison are two nearby, low-mass pre-MS systems that also display evidence for highly inclined disks: 2MASS J12014343–7835472 (henceforth 2M1201–78) and TWA 30B. 2M1201–78 is an early M-type star ($\sim M2.25$) that is also a member of the ~ 5 Myr ϵ CA (Luhman 2004; Dickson-Vandervelde et al. 2021). As well as hosting a highly inclined disk ($i \sim 84^{\circ}$), optical spectroscopy showed some signs of ongoing accretion in the form of emission from lines of He I, [S II], and the Ca II triplet, although other signatures were not detected. Modeling by Fang et al. (2013) attributes the lack of some accretion signatures to a sparse inner disk.

A known member of the TW Hya association (~ 8 Myr), TWA 30B is an M-type (M3/M4) pre-MS star that is a wide-separation (~ 3400 au) companion to TWA 30A (Looper et al. 2010). Like the 2M1155–79AB system, TWA 30B is fainter than its companion TWA 30A in the optical and NIR; it is 5 mag fainter than TWA 30A despite having a slighter earlier spectral type. The TWA 30B disk has been detected via its WISE excess emission and ALMA submillimeter continuum emission (Schneider et al. 2012; Rodriguez et al. 2015). Optical and NIR spectra of TWA 30B show not only He I emission lines but also multiple forbidden lines (such as [O I], [O II], and [C I]), indicating that the system is actively accreting and likely drives jets (Looper et al. 2010).

In Figure 5, we compare the SEDs of 2M1155–79B, 2M1201–78, and TWA 30B, as compiled from data from Gaia EDR3, 2MASS, VHS, and WISE. The SEDs are overlaid with composite blackbody curves approximating the stars’ photospheric and disk emission (dashed lines). Only the photometric data for 2M1155–79B have been dereddened; the ϵ CA region toward 2M1201–78 appears to show minimal interstellar reddening (Murphy et al. 2013), while the TWA 30B system displays variable reddening due to its dusty circumstellar disk (Looper et al. 2010; Principe et al. 2016).

While the three objects are similar in nature—i.e., low-mass stars with large IR excesses—the comparison of their SEDs indicates that there are important differences in either disk structure or disk inclination. TWA 30B has a flat SED, indicative of a “full” disk with no significant inner cavity, while 2M1201 appears to have a clear break between its photospheric and disk emission, indicative of an inner disk cavity, as hypothesized by Fang et al. (2013). This is consistent with the accretion signatures from the two objects: 2M1201 has weaker accretion signatures than TWA 30B (Looper et al. 2010; Fang et al. 2013). However, small differences in disk inclination could also explain these differences in SEDs. Because of WISE’s inability to cleanly resolve 2M1155–79B from A, we are unable to establish which of these contrasting SED shapes might best characterize 2M1155–79B.

Figure 6 compares the NIR spectra of 2M1155–79B and TWA 30B (previously classified as M4; Looper et al. 2010; Principe et al. 2016), including the strengths of the He I $1.083\ \mu\text{m}$ emission lines. The TWA 30B IRTF-SpeX spectrum (obtained on 2011 June 8) was among the NIR spectra presented in Principe et al. (2016) least affected by the variable reddening of TWA 30B. The comparison supports our determination of a mid- to late M spectral type for 2M1155–79B (Section 3.1). The $1.083\ \mu\text{m}$ He I line EWs of the two systems are similar: we measure $\sim -20\ \text{\AA}$ for

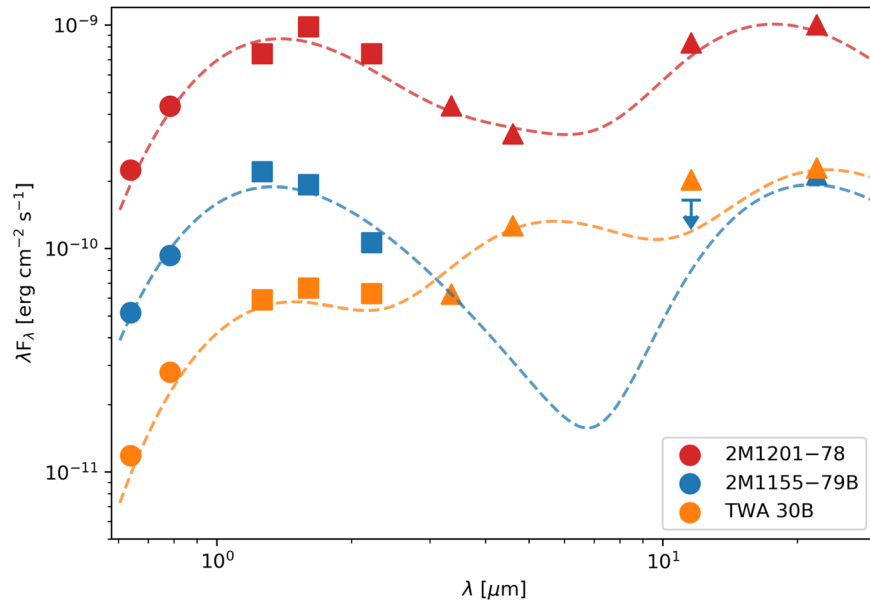


Figure 5. The SEDs of 2M1155–79B (in blue), TWA 30B (in orange), and 2M1201–78 (in red) displayed on a log–log scale. The data markers are indicative of the same photometric bands as listed in the caption of Figure 4. The fluxes of all three systems have been normalized to a uniform distance of 10 pc. The dashed lines indicate the combined blackbody model for each system. The stellar photospheres are modeled as simple blackbodies and are not indicative of the actual stellar effective temperatures. The photospheric blackbodies for each system, scaled to the H -band flux, are 2750 K for 2M1155–79B, 2500 K for TWA 30B, and 2650 K for 2M1201–78. The remaining excesses (corresponding to the disks) are modeled using two blackbodies for 2M1201–78 ($T = 200, 750$ K) and TWA 30B ($T = 150, 620$ K; Rodriguez et al. 2015) and a single blackbody for 2M1155–79B ($T = 170$ K).

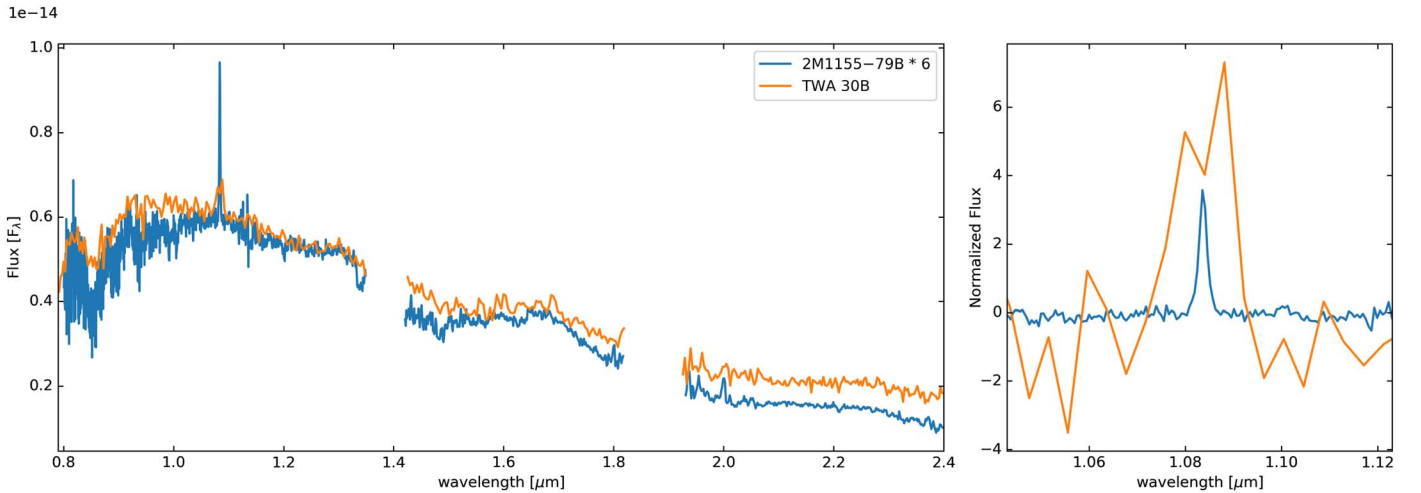


Figure 6. Two IR spectra are displayed in both panels: 2M1155–79B (blue, taken with the FIRE instrument) and TWA 30B (orange, taken with the SPeX instrument). In the left panel, the 2M1155–79B spectrum has been normalized for visualization with the TWA 30B spectrum by the entire spectrum being multiplied by a constant of 6 and shows the full wavelength coverage. The right panel is centered on the He I 1.083 emission line, and both fluxes have had the continuum flux subtracted and normalized to 0.

TWA 30B, versus $\sim 12 \text{ \AA}$ for 2M1155–79B (Section 3.1). The line is unresolved in both spectra, so we are unable to compare the line widths.

As noted in Section 4.1, the apparent optical/NIR photometric and color variability of 2M1155–79B suggests that it experiences variable obscuration by its highly inclined disk; curiously, this behavior more closely resembles that of TWA 30B’s wide-separation companion, TWA 30A, than TWA 30B itself (Looper et al. 2010; Principe et al. 2016). The disk surrounding TWA 30A is most likely less highly inclined than its companion, as TWA 30A is brighter in the optical/NIR and, unlike TWA 30B, has been detected in X-rays (Looper et al. 2010; Principe et al. 2016).

Another recently discovered low-mass pre-MS star pair in which (like 2M1155–79AB) one component harbors a disk and one is diskless is the potential wide binary DENIS-P J1538316–103900 (DENIS1538–1039) and DENIS-P J1538317–103850 (DENIS1538–1038). DENIS1538–1038 is a ~ 1 Myr old brown dwarf (spectral type M5.5) with an IR excess indicative of a disk (Nguyen-Thanh et al. 2020). The M3 star DENIS1538–1039 is seen at $10''$ projected separation from DENIS1538–1038. Nguyen-Thanh et al. (2020) conclude that the two stars are potential members of the Upper Scorpius association, although (as noted by Nguyen-Thanh et al. 2020), at an estimated age of ~ 1 –5 Myr, they are much younger than the average age of the association (~ 10 Myr; Luhman & Esplin 2020); they are also far

from the main Upper Scorpius association complex, further casting their membership in doubt. On the basis of Gaia DR2 data, Nguyen-Thanh et al. (2020) concluded that the pair represent a chance line-of-sight alignment of two members of the same NYMG. However, in Gaia EDR3, the two components have the same proper motions and parallaxes within the uncertainties, indicating that the two stars are in fact a wide binary analogous to 2M1155–79AB, i.e., a wide-separation pair of young M stars near the stellar/substellar boundary, one with a disk and one without.

Two other systems merit mention here, as potential younger analogs to the 2M1155–79AB wide binary. Like 2M1155–79B, the companion to the 1–2 Myr old 2MASS J19005804–3645048 was initially thought to be a planet-mass object before follow-up spectroscopy instead suggested that the star was a young late M dwarf (Christiaens et al. 2021). Christiaens et al. (2021) discuss the implication that the companion is an obscured low-mass star for which only a small fraction of its light emerges owing to an edge-on disk, as well as the possibility that the companion is an accreting protoplanet that is being heated by accretion shocks. It is unlikely that 2M1155–79B falls into this second category, given the lack of WISE detection of warm dust around 2M1155–79A (Section 3.2). The second system, HK Tau AB, is a low-mass, wide binary in the Taurus star-forming region that, like 2M1155–79AB, consists of two stars of similar (in this case, early M) spectral type, but with B many magnitudes fainter than A (Monin et al. 1998). NIR imaging of the system revealed that HK Tau B is occulted by an edge-on disk (Stapelfeldt et al. 1998). Subsequent scattered light and submillimeter observations demonstrate that both components possess extensive gas and dust disks, but with sharply contrasting inclinations ($i \sim 43^\circ$ and $i \sim 85^\circ$, respectively; McCabe et al. 2011; Jensen & Akeson 2014).

It is also worth considering whether 2M1155–79AB and some of the aforementioned systems constitute examples of young, hierarchical multiples wherein at least one component harbors a relatively long-lived, dusty disk (Kastner 2018, and references therein). There are multiple instances of circumbinary disks in such systems, as well as young hierarchical multiple systems showing the presence of disks around some components and not others; the HD 104237 system within ϵ CA is an example of a particularly complex system with both of these characteristics (Murphy et al. 2013; Dickson-Vandervelde et al. 2021). Thus far, however, there is no evidence that 2M1155–79AB is such a (hierarchical) multiple system (in particular, DR2 photometry is consistent with 2M1155–79A being a single star; Dickson-Vandervelde et al. 2021).

4.3. The Nature of 2M1155–79B

While the original evidence in Dickson-Vandervelde et al. (2020) pointed toward 2M1155–79B being a nascent, 10 M_J planet, the spectral type determined here, M5/6, is inconsistent with this picture. Nonetheless, 2M1155–79B is potentially still near the hydrogen-burning limit; pre-MS model evolutionary tracks place the stellar versus brown dwarf boundary around a spectral type of M6 at 3–5 Myr (Baraffe et al. 2015). A firm conclusion as to the fate of 2M1155–79B—low-mass star or brown dwarf—will require optical spectroscopy to confirm the spectral type of this enigmatic system.

To our knowledge, 2M1155–79B is the latest M-type pre-MS star in which the He I 1.083 μm emission line has yet been

detected. In higher-mass pre-MS (T Tauri) stars, this line is a sensitive probe of accretion shocks and accretion-driven winds (Kwan et al. 2007), manifested in the form of red- and blueshifted absorption features that are a consequence of the high 1.083 μm line opacity (Edwards et al. 2006; Kwan & Fischer 2011; Sousa et al. 2021). For a high-inclination star–disk system with stellar and/or disk winds, the He I 1.083 μm emission has a narrow, blueshifted absorption feature owing to the emission passing through the slow disk wind component (Kwan et al. 2007). Given the resolution of our spectra, we cannot retrieve any information about potential blueshifted absorption; however, the EW of the emission line from 2M1155–79B is similar to that of mid-K classical T Tauri star disks (Edwards et al. 2003), and our initial modeling supports the presence of a nearly edge-on circumstellar disk in the system (Figure 4). Modeling by Kwan & Fischer (2011) indicates that He I emission could be arising from the accretion flow close to a stellar impact shock, resulting in UV photoionization and temperatures of at least 10^4 K. However, since 2M1155–79B has a much lower mass and therefore should have a lower shock temperature than in the Kwan & Fischer (2011) models, the He I 1.083 μm could be indicative of the presence of a large-scale wind or jet. NIR imaging of this object might reveal a jet origin for the He I 1.083 μm emission, while higher-resolution spectroscopy of the He I 1.083 μm emission will allow for analysis of intervening kinematic structures through the study of potential absorption components within the line profile. The large EW of this line in the spectrum of 2M1155–79B makes this object a strong candidate for the use of both of these methods.

5. Conclusions

The object 2M1155–79B is a low-mass member of the ~ 5 Myr moving group ϵ CA and a wide-separation companion ($5''.75$, 580 au) to another ϵ CA member, 2M1155–79A. The SED of 2M1155–79B is ~ 10 –100 times fainter than 2M1155–79A throughout the optical and NIR (Figures 1 and 4). The extreme faintness and redness of 2M1155–79B in Gaia DR2 and archival 2MASS photometry presented the scenario that 2M1155–79B was a planet-mass object ($M \sim 10 M_J$). However, we have obtained NIR spectroscopy with Magellan/FIRE demonstrating that the object is best matched by a young star standard spectra in the range M5–M6 (Figure 1). The fact that 2M1155–79B is much fainter in the optical and NIR than expected of a star of this spectral type is hence most likely due to partial occultation of the stellar photosphere by a highly inclined circumbinary disk. Furthermore, a strong He I 1.083 μm emission line is observed in the FIRE spectra of 2M1155–79B, indicative of ongoing accretion and accretion-driven winds and/or jets (see Section 4.3). Nevertheless, the FIRE spectra of 2M1155–79B and 2M1155–79A are very similar in shape, revealing that the two stars may be nearly twins, both with spectral types in the range M5–M6. The spectral type we infer for 2M1155–79A from its FIRE spectrum is somewhat later than that previously determined from its optical spectrum. Follow-up optical spectroscopy of 2M1155–79B is needed to clarify the photospheric properties of 2M1155–79B and verify that the two components of the 2M1155–79AB binary are indeed nearly twins. Analysis of the WISE photometry for the 2M1155–79AB system (Section 3.2, Figure 3) demonstrates that the infrared excess originally associated with 2M1155–79A instead originates from 2M1155–79B, supporting the

interpretation that the secondary is orbited and occulted by a dusty disk. Modeling of the SED of the 2M1155–79B star–disk system (Figure 4) shows that a highly inclined disk ($i \sim 75^\circ\text{--}81^\circ$) can account for the flux difference between primary and secondary.

As discussed in Section 4.2, these results place 2M1155–79B among a small subset of pre-MS, low-mass stars that both are highly obscured by edge-on disks and show signs of active accretion. Like these other, analogous systems, the 2M1155–79B system is a particularly promising subject for studies of star and planet formation around low-mass stars.

We thank the anonymous referee for helpful comments and suggestions. This research is supported by NASA Exoplanets Program grant 80NSSC19K0292 to Rochester Institute of Technology. This work has made use of data from the European Space Agency (ESA) mission Gaia (<https://www.cosmos.esa.int/gaia>), processed by the Gaia Data Processing and Analysis Consortium (DPAC, <https://www.cosmos.esa.int/web/gaia/dpac/consortium>). Funding for the DPAC has been provided by national institutions, in particular the institutions participating in the Gaia Multilateral Agreement. This publication makes use of data products from the Two Micron All Sky Survey, which is a joint project of the University of Massachusetts and the Infrared Processing and Analysis Center/California Institute of Technology, funded by the National Aeronautics and Space Administration and the National Science Foundation. This publication makes use of data products from the Wide-field Infrared Survey Explorer, which is a joint project of the University of California, Los Angeles, and the Jet Propulsion Laboratory/California Institute of Technology, funded by the National Aeronautics and Space Administration.

ORCID iDs

D. Annie Dickson-Vandervelde  <https://orcid.org/0000-0002-4555-5144>
 Joel H. Kastner  <https://orcid.org/0000-0002-3138-8250>
 Jonathan Gagné  <https://orcid.org/0000-0002-2592-9612>
 Adam C. Schneider  <https://orcid.org/0000-0002-6294-5937>
 Jacqueline Faherty  <https://orcid.org/0000-0001-6251-0573>
 Emily C. Wilson  <https://orcid.org/0000-0002-3947-5586>
 Christophe Pinte  <https://orcid.org/0000-0001-5907-5179>
 Francois Ménard  <https://orcid.org/0000-0002-1637-7393>

References

Allers, K. N., & Liu, M. C. 2013, *ApJ*, 772, 79
 Bailer-Jones, C. A. L., Rybizki, J., Foesneau, M., Demleitner, M., & Andrae, R. 2021, *AJ*, 161, 147
 Baraffe, I., Homeier, D., Allard, F., & Chabrier, G. 2015, *A&A*, 577, A42
 Bochanski, J. J., Hennawi, J. F., Simcoe, R. A., et al. 2009, *PASP*, 121, 1409
 Cardelli, J. A., Clayton, G. C., & Mathis, J. S. 1989, *ApJ*, 345, 245
 Christiaens, V., Ubeira-Gabellini, M.-G., Cánovas, H., et al. 2021, *MNRAS*, 502, 6117

Cushing, M. C., Vacca, W. D., & Rayner, J. T. 2004, *PASP*, 116, 362
 D’Alessio, P., Calvet, N., Hartmann, L., Franco-Hernández, R., & Servín, H. 2006, *ApJ*, 638, 314
 Dickson-Vandervelde, D. A., Wilson, E. C., & Kastner, J. H. 2020, *RNAAS*, 4, 25
 Dickson-Vandervelde, D. A., Wilson, E. C., & Kastner, J. H. 2021, *AJ*, 161, 87
 Edwards, S., Fischer, W., Hillenbrand, L., & Kwan, J. 2006, *ApJ*, 646, 319
 Edwards, S., Fischer, W., Kwan, J., Hillenbrand, L., & Dupree, A. K. 2003, *ApJL*, 599, L41
 Fang, M., van Boekel, R., Bouwman, J., et al. 2013, *A&A*, 549, A15
 Fitzpatrick, E. L., Massa, D., Gordon, K. D., Bohlin, R., & Clayton, G. C. 2019, *ApJ*, 886, 108
 Furlan, E., Luhman, K. L., Espaillat, C., et al. 2011, *ApJS*, 195, 3
 Gagné, J., & Faherty, J. K. 2018, *ApJ*, 862, 138
 Gaia Collaboration, Brown, A. G. A., Vallenari, A., et al. 2021, *A&A*, 649, A1
 Gaia Collaboration, Prusti, T., de Bruijne, J. H. J., et al. 2016, *A&A*, 595, A1
 Jensen, E. L. N., & Akeson, R. 2014, *Natur*, 511, 567
 Kastner, J. H. 2018, *RNAAS*, 2, 137
 Kastner, J. H., Rapson, V., Sargent, B., Smith, C. T., & Rayner, J. 2015, in 18th Cambridge Workshop on Cool Stars, Stellar Systems, and the Sun, ed. G. van Belle & H. C. Harris (Flagstaff, AZ: Lowell Observatory), 313
 Kastner, J. H., Stelzer, B., & Metchev, S. A. (ed.) 2016, in IAU Symp. 314, Young Stars & Planets Near the Sun (Cambridge: Cambridge Univ. Press), doi:10.1017/S1743921315006699
 Kastner, J. H., Thompson, E. A., Montez, R., et al. 2012, *ApJL*, 747, L23
 Kwan, J., Edwards, S., & Fischer, W. 2007, *ApJ*, 657, 897
 Kwan, J., & Fischer, W. 2011, *MNRAS*, 411, 2383
 Lagrange, A.-M., Langlois, M., Gratton, R., et al. 2016, *A&A*, 586, L8
 Lallement, R., Babusiaux, C., Vergely, J. L., et al. 2019, *A&A*, 625, A135
 Lodieu, N., Hambly, N. C., & Cross, N. J. G. 2021, *MNRAS*, 503, 2265
 Looper, D. L., Bochanski, J. J., Burgasser, A. J., et al. 2010, *AJ*, 140, 1486
 Luhman, K. L. 2004, *ApJ*, 616, 1033
 Luhman, K. L., & Esplin, T. L. 2020, *AJ*, 160, 44
 Luhman, K. L., Mamajek, E. E., Shukla, S. J., & Loutrel, N. P. 2017, *AJ*, 153, 46
 McCabe, C., Duchêne, G., Pinte, C., et al. 2011, *ApJ*, 727, 90
 McMahon, R. G., Banerji, M., Gonzalez, E., et al. 2013, *Msngr*, 154, 35
 Monin, J. L., Menard, F., & Duchene, G. 1998, *A&A*, 339, 113
 Murphy, S. J., Lawson, W. A., & Bessell, M. S. 2013, *MNRAS*, 435, 1325
 Nguyen-Thanh, D., Phan-Bao, N., Murphy, S. J., & Bessell, M. S. 2020, *A&A*, 634, A128
 Pecaut, M. J. 2016, in IAU Symp. 314, Young Stars & Planets Near the Sun, ed. J. H. Kastner, B. Stelzer, & S. A. Metchev (Cambridge: Cambridge Univ. Press), 85
 Pecaut, M. J., & Mamajek, E. E. 2013, *ApJS*, 208, 9
 Pinte, C., Harries, T. J., Min, M., et al. 2009, *A&A*, 498, 967
 Pinte, C., Ménard, F., Duchêne, G., & Bastien, P. 2006, *A&A*, 459, 797
 Principe, D. A., Sacco, G., Kastner, J. H., Stelzer, B., & Alcalá, J. M. 2016, *MNRAS*, 459, 2097
 Rodet, L., Beust, H., Bonnefoy, M., et al. 2019, *A&A*, 631, A139
 Rodriguez, D. R., van der Plas, G., Kastner, J. H., et al. 2015, *A&A*, 582, L5
 Sacco, G. G., Kastner, J. H., Forveille, T., et al. 2014, *A&A*, 561, A42
 Schlafly, E. F., Meisner, A. M., & Green, G. M. 2019, *ApJS*, 240, 30
 Schneider, A., Melis, C., & Song, I. 2012, *ApJ*, 754, 39
 Skrutskie, M. F., Cutri, R. M., Stiening, R., et al. 2006, *AJ*, 131, 1163
 Sousa, A. P., Bouvier, J., Alencar, S. H. P., et al. 2021, *A&A*, 649, A68
 Stapelfeldt, K. R., Krist, J. E., Menard, F., et al. 1998, *ApJL*, 502, L65
 Vacca, W., Cushing, M., & Rayner, J. 2003, *PASP*, 115, 389
 Wright, E. L., Eisenhardt, P. R. M., Mainzer, A. K., et al. 2010, *AJ*, 140, 1868
 Wu, Y.-L., Close, L. M., Bailey, V. P., et al. 2016, *ApJ*, 823, 24
 Wu, Y.-L., Close, L. M., Males, J. R., et al. 2015a, *ApJ*, 801, 4
 Wu, Y.-L., Close, L. M., Males, J. R., et al. 2015b, *ApJL*, 807, L13